ARTICLES

Complex Nature of the UV and Visible Fluorescence of Colloidal ZnO Nanoparticles

S. Monticone, R. Tufeu, and A.V. Kanaev*

Laboratoire d'Ingénierie des Matériaux et des Hautes Pressions, CNRS, Villetaneuse, France

Received: October 22, 1997; In Final Form: February 2, 1998

Time-resolved spectroscopy of colloidal ZnO nanoparticles has been carried out with a laser excitation at 248 nm. UV and visible fluorescence has been analyzed. Except for the known *band gap* 370-nm and *impurity* 510-nm emissions, we have found additional continua at ∼300, 430, and 545 nm. These continua were developed in solutions of different composition, with excess Zn^{2+} and OH^- ions, and in function of time. All but 510-nm fluorescence bands exhibit short nanosecond or subnanosecond decays. The green fluorescence at 510 nm originating from 4-nm particles in Zn^{2+}-rich solutions is a much longer-lived, 1.0 μs. The band natures are discussed. Cluster size distribution and growth kinetics have been recovered from spectral measurements.

Introduction

Semiconductor nanoparticles have been under continuous scientific interest since the 80s because of their unique quantum nature, which changes the material solid-state properties.[1−3] The possibility of artificial adjustment of bulk material properties by varying the size, structure, and composition of constituting nanoscale particles makes them a candidate for a multiple important applications in the field of a new material research.[4]

Optical methods give rich experimental information about an energetical structure of these finite-size solids. Principal understanding of size-dependent optical properties of semiconductor clusters has been achieved in a number of theoretical publications for a long time.[5−7] An electronic excitation in semiconductor clusters consists of a loosely bound electron−hole pair that is generally delocalized over a nanoparticle. In this case the lowest energy level (where the pair obeys a minimum kinetic energy) and therefore the semiconductor band gap increase when the cluster size diminishes. Development of methods of preparation and stabilization of monodispersed semiconductor nanoparticles in transparent colloids offers a nice opportunity of experimental verification of theoretical predictions.

In this article we present a spectroscopical observations of colloidal solution of ZnO nanoparticles. ZnO is one of the representatives of the class metal oxides, which are of importance in electrochemistry and catalysis. ZnO solid has a band gap energy of ∼3 eV and therefore can be analyzed by spectroscopical methods in most of the solvents (like methanol, propan-2-ol, water) that are transparent in the whole UV−visible spectral regions. Methods of preparation and long-term stabilization of ZnO colloidal solutions are already available in the literature. In complement to the earlier published data,[9−12] with our 248-nm laser excitation we have found new peculiarities of the fluorescence spectra that are consistent with the nanoparticles size distribution and the environment: excess Zn^{2+} or OH^- ions. We present a correlation analysis between the particles' (*nano*)size and spectroscopic observations, which can allow us to control the kinetics at the early stage of the particles growth.

Experiment

To conduct studies on time-resolved spectroscopy of semiconductor clusters, we have developed an experimental setup, which includes a laser source of sample excitation, sample chamber, and analyzing system. A standard KrF excimer laser supplies pulses of 20-ns duration and of energy varying from 150 mJ down to the microjoule level with a rate up to 10 Hz. Laser energy is measured with a EM500 joulemeter by Optronix. The optical system supplies the canalized laser beam to the sample holder closed in a dark chamber. We have used a window-free metallic (Al) holder to escape parasite fluorescence. In such a case a very low intensity signal could be observed. For the moment, we did not vary the sample temperature, which was maintained at 25 °C. The registration system consists of two parts. (i) Spectra are analyzed by a Peltier cooled intensified CCD camera by Princeton Instruments coupled with a Cromex motorized 250-mm monochromator equipped with three gratings: 150 (UV/vis), 300 (UV), and 1200 (vis) Gr./mm. Fluorescence from the sample chamber was transferred by three fiber optical branches. This allows us to record time-resolved spectra simultaneously from three different points of an excitation volume and with a time window as small as 5 ns, delayed after a laser pulse with an increment of 1 ns. Spectra were calibrated by a finger Hg lamp (ORIEL). (ii) For registration of a fluorescence decay we have used a Hamamatsu Photonics fully integrated fast (rise-time 0.65 ns) photomultiplier (PMT) H5783-04 sensitive in a 180−900-nm spectral range and a 500-MHz TDS510 digitizing oscilloscope by Tektronix. The registration system was triggered either by a laser pulse or by an external pulse generator. The last case allows a wider range of synchronization but has the disadvantage of lower temporal

* Author to whom correspondence should be addressed.

S1089-5647(97)03425-1 CCC: $15.00
Published on Web 03/31/1998

resolution because of the laser pulse jitter. The experimental system allows a full computer control.

An excellent S/N ratio in the registration of spectra was achieved with a -30 °C detector cooling. This allowed us to accumulate spectra and decay curves typically in a 50 laser shots, though longer expositions were performed if necessary. Subtraction of a background noise was made in each case before proceeding the spectra. Because of a rather strong fluorescence of our samples, no extra amplification of the signal was applied after PMT.

Nanoparticles of ZnO were prepared by a method described in ref 11. In short, two kinds of colloids were prepared: with excess Zn^{2+} or OH^- ions. We shall call them below ZnO(1) and ZnO(2) samples, respectively.

ZnO(1) (Excess Zn^{2+} Ions). First, two solutions A and B were made: (A) 37.7 mg of zinc perchlorate salt $Zn(ClO_4)_2 \cdot 6H_2O$ was diluted in 40.5 mL of methanol and added under strong stirring to a mixture of 9×10^{-3} M NaOH in 40.5 mL of methanol; (B) 0.7 mL of 0.2 M solution of $Zn(ClO_4)_2 \cdot 6H_2O$ in methanol is mixed under strong stirring with 0.5 mL of water and 10 mL of methanol. To prepare the ZnO(1) sols two solutions A and B were mixed, complemented with a methanol until 100 mL, stirred overnight at 25 °C, and subsequently stored in a dark container at room temperature. Initially opalescent solution became completely transparent the next morning. The mixture containing slowly growing ZnO nanoparticles was stable from hours to weeks depending on small deviations from a standard procedure of preparation. In a certain case, even after 2 months, despite a very light white deposit on the container walls, the presence of suspended ZnO nanoparticles was evidenced in the mixture.

ZnO(2) (Excess OH^- Ions). The method of preparation of ZnO(2) colloids was substantially similar to the method described above. The only difference concerned the B solution, which did not contain zinc perchlorate salt.

The concentration of ZnO varied in the range $(1-4) \times 10^{-3}$ M. Generally, samples with a higher ZnO concentration were less stable, and particles grew and precipitated rapidly. The concentration of the excess ions Zn^{2+} or OH^- was varied in the ranges between 10^{-4} and 4×10^{-4} M or 2×10^{-4} and 1.2×10^{-2} M, respectively. Some excess ions concentration was necessary for the colloid stability.

Particles size was controlled by the onset of absorption spectra, which undergoes a red shift when particles grow. In the limit of $R_{\text{particle}} \rightarrow \infty$, the absorption starts at 3.44 eV (360.4 nm), which is characteristic of ZnO solids. This method is well-characterized in literature for quasi-monodispersed nanoparticles. Additionally, electron microscopy was also used for a verification of some absorption measurements.

Results and Discussion

I. Calculation of the Calibration Curve: Size/Band Gap Energy. Presently, results of different indirect methods of particle size determination are used to compare with results of transmission electron microscopy (TEM). The last method is generally considered as giving the true histograms. Below we will discuss a spectroscopical method for a mean particle size determination.

There are several approaches to estimate a particle's size (size $\equiv$ 2R) from the absorption onset. Brus[7] has derived an analytical formula based on effective mass approximation ($m_{e,h}$ = const): $E_g = E_g^{(s)} + (\pi^2/R^2) - (3.6/R)$, where the cluster and solid-state band gap energies E_g and $E_g^{(s)}$ and cluster radius R are respectively expressed in the rydberg ($Ry = (\mu e^4)/(2\epsilon^2\hbar^2)$) and bohr ($(\epsilon\hbar^2)/(\mu e^2)$) units. Here $\mu^{-1} = m_e^{-1} + m_h^{-1}$ is the exciton reduced mass and ϵ is the dielectric constant of a semiconductor. Generally, it is accepted that in ZnO solid $\epsilon =$ 3.7 and the effective masses of an electron and a hole expressed in free electron mass are 0.24 and 0.45, although higher values measured directly in nanoparticles, 0.3 ± 0.1 and 0.8 ± 0.5, have been recently reported in ref 15. We have chosen the first set of values and $E_g^{(s)} = 3.44$ eV from ref 6, which gave the units of $Ry = 156$ meV and $a_B = 1.25$ nm. The calibration using this approach is given by curve a in Figure 1a. Another approach based on quantum mechanical variational calculation have been described by Kayanuma in ref 16. It is presented by a curve b in Figure 1a.

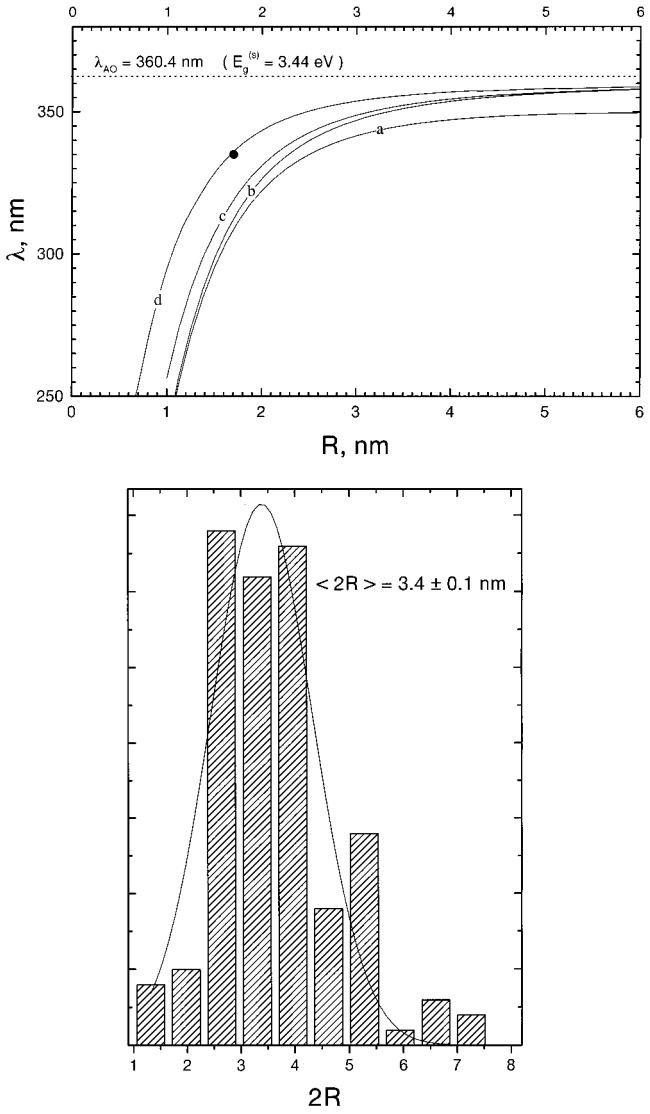

Figure 1. (a) Calibration curves $\lambda_{\text{onset}}(R)$: according to the Brus formula[6] (a), according to Kayanuma's variational calculations[16] for an infinite barrier height (b), taking a barrier height of 4.3 eV (c), and our calculation using an effective mass correction (d). Experimental point (●) is given from (b). (b) TEM histogram of the freshly prepared ZnO(1) sample (the corresponding absorption onset is at 335 nm).

In both cases an infinite potential barrier has been placed on the nanoparticle surface. This effectively holds an exciton inside the particle and therefore overestimates its kinetic energy at small radii. As it was shown in ref 17, a better approach can be obtained by considering a finite well barrier. A barrier height of $U_b = 3.8$ eV has been chosen in refs 11 and 17. We have carried a quantum mechanical variational calculation using a

value of $U_b = 4.3$ eV from ref 18. The result is shown by curve c in Figure 1a. As expected, this curve coincides with curve b in the limit of large radii but deviates from it and from curve a given by the Brus formula at smaller sizes. Finally, good coincidence with experiment gives another particle-in-the-box model calculation described in ref 19. Here the hole was fixed in the cluster center, and a particle with a reduced mass μ was considered to move in its Coulomb potential limited by the cluster walls ($U_b = \infty$).

Nevertheless, these models overestimate the mean cluster size obtained from the absorption onset. As was shown in refs 11 and 17 for the example of CdS and ZnO solids, the results obtained by this method correlate with particle sizes obtained by extrapolating the steep part of the TEM histogram. In the case of size distributions presented in ref 11 for ZnO, the particle size obtained from the absorption onset has deviated roughly by 25% from the TEM curve maximum.

Certainly, there are several reasons why these models could not work well in the limit of small sizes: (i) breakdown of an effective mass approximation, (ii) reducing of the effective dielectric constant, and (iii) changes in the solid structure of a small particle. The problem can be solved in principle, by knowing the full $E(\bar{k})$ curve from the band structure calculations. An empirical pseudopotential method as developed in ref 20 gives a very good agreement with experiment over a wide range of cluster sizes. Another approach was proposed by Wang in ref 21, where two theoretical models have been developed: hyperbolic band and LCAO-MO (tight binding). Both models include the effect of band nonparabolicity and also gave a very good agreement with experiment down to cluster diameters of 2 nm (PbS).

In our work in light of the above discussion, for a mean cluster size determination we have introduced a very simple model correction for the (e, h) effective masses increase in small particles. We used variational quantum mechanical calculations of the type described in ref 16. First, we have considered free motion of a hole (inside the particle with the effective mass $m_h = 0.45m_0$) and of an electron (inside, with $m_e = 0.24m_0$; outside, with free electron mass m_0), bound by Coulomb interaction in a finite potential well of 4.3 eV. Dielectric constants of ZnO and of surrounding liquid of 3.7 and 1.8 (methanol) were used. Second, we used a LCAO-MO approach for a description of a band structure, which allowed us to estimate the effective masses as $m_{e,h}(k) = m_{e,h}(0)/\cos(ka)$, where the lattice constant of ZnO of $a = 0.541$ nm has been used. The result of this calculation is given by solid curve d in Figure 1a. We will use this calibration curve d to obtain particle sizes from spectroscopical measurements: (i) of the absorption onset (Section II.A) and (ii) of the fluorescence spectra (Section III).

II. ZnO Spectroscopy. In the present study we have measured absorption and fluorescence spectra and fluorescence decay curves of ZnO nanoparticles excited with 248-nm laser pulses. To avoid charging of particles by photogenerated electrons, which leads to changes in spectra, which has been already described in ref 9, we maintained low repetition rate of 2 Hz and relatively low energy density of $E_L \leq 5$ mJ/cm^2 of laser pulses. In this range of experimental conditions spectra were stable and reproducible. A typical example of absorption and fluorescence spectra recorded with freshly prepared ZnO-(1) sample is given in Figure 2.

A. Absorption. It is known that intensities I_t and I_0 of transmitted and incident light are related by $I_t = I_0 \cdot \exp(-\alpha L)$, where α is an absorption coefficient. ZnO is a direct-band semiconductor for which α is related to the excitation

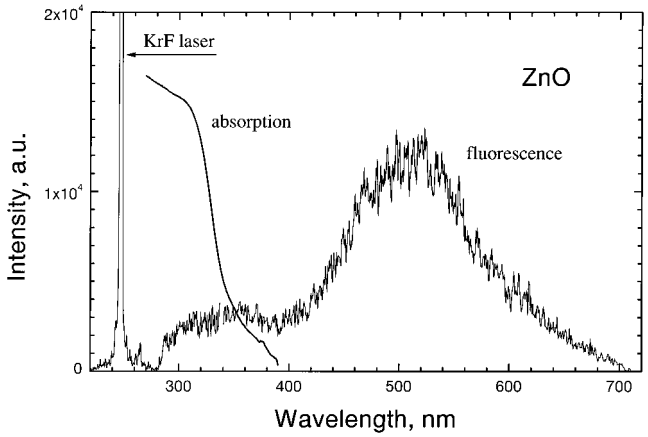

Figure 2. Typical example of the absorption and fluorescence spectra recorded in freshly prepared ZnO(1) sample.

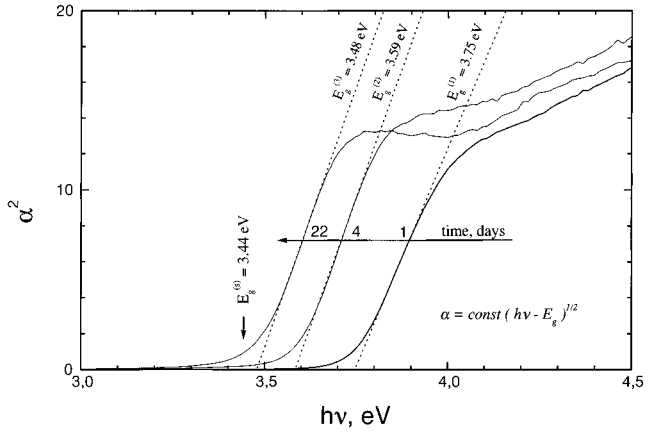

Figure 3. Shift of the onset of absorption spectra of ZnO(1) sample 1, 4, and 22 days after preparation.

energy ($E_{exc} = h\nu$) by $\alpha = \text{const} \cdot (h\nu - E_g)^{1/2}$ (for $h\nu \geq E_g$),[13] where E_g is a band gap energy. Therefore, to obtain the absorption onset we plotted $\ln^2(I_t/I_0)$ versus energy $h\nu$. Extrapolation of the linear part until it intersects the $h\nu$-axis gives E_g. Such plots for the same ZnO(1) sample 1, 4, and 22 days after preparation are shown in Figure 3. Below the absorption onset one can see a long-wave tail of approximately exponential form, which obeys Urbach's rule:[14] $\alpha = \alpha(E_g) \cdot \exp[\sigma/kT(E - E_g)]$, where σ is a constant. It originates from the sub-bandgap phonon assisted optical transitions.

In all our freshly prepared ZnO(1) samples (1 night after the preparation starts) at [ZnO] $= 2 \times 10^{-3}$ M the absorption onset wavelength was at $\lambda_{AO} = 330$ nm (3.75 eV). According to our calibration curve this corresponds to a size of 3.0 nm. Particles of this size have been found in the majority of these solutions. The TEM histogram corresponding to $\lambda_{AO} = 3.70$ eV and showing a maximum at $2R = 3.4$ nm is presented in Figure 1b. This point is in a good agreement with the calculated calibration curve d in Figure 1a. We did not verify in the present study in a systematic way the correspondence of the calculated calibration curve to the measured one. Such correlation analysis has been already done in previous publications.[11,17] In the present article in Section III we will compare the results obtained from our measurements of the absorption and fluorescence spectra.

The colloidal nanoparticles slowly grow with time, attaining $R = 5$ nm after a period of almost 2 months. After this time absorption spectra were little sensitive to changes in size showing the absorption onset close to 3.44 eV corresponding to the ZnO solid. Size variation of ZnO(1) particles with time measured by this method is presented in Figure 4.

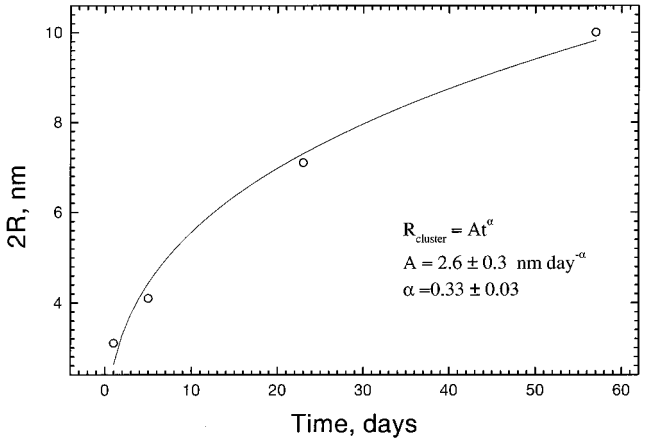

Figure 4. Dependence of ZnO(1) particle size on time.

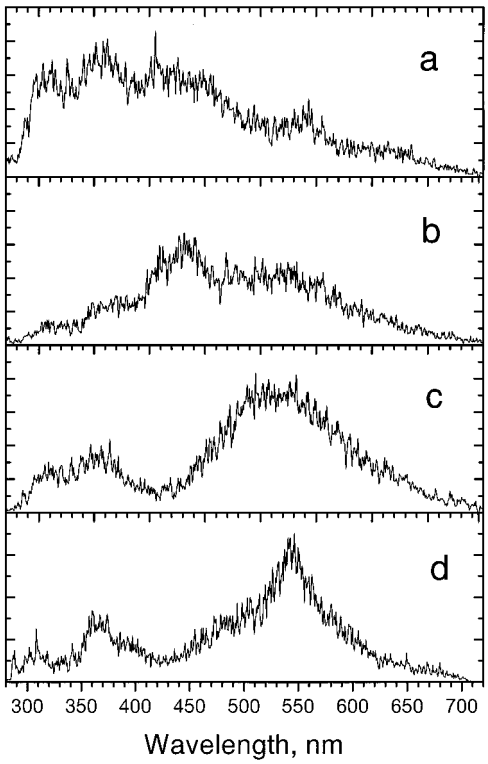

Figure 5. Fluorescence spectra recorded in different stable (a, c) and slightly precipitated (b, d) colloids: $[OH^-] = 1.2 \times 10^{-3}$ M, [ZnO] = 4×10^{-3} M, 1 day after preparation (a); $[OH^-] = 2.4 \times 10^{-4}$ M, [ZnO] = 1.8×10^{-3} M, 12 days after preparation (b); $[Zn^{2+}] = 1 \times 10^{-3}$ M, [ZnO] = 4×10^{-3} M, 2 days after preparation (c); $[Zn^{2+}] = 4 \times 10^{-4}$ M, $[Zn^{2+}] = 2 \times 10^{-3}$ M, 30 days after preparation (d).

B. Fluorescence. If we compare absorption and fluorescence spectra presented in Figure 2, one can easily identify the UV emission band to a direct *band gap* transition .[9] As has been remarked before in old samples, it is placed at ~375 nm, shifted by $\sim 10^2$ meV, respectively, to the absorption onset (360.5 nm). UV spectra recorded in different ZnO(1) or ZnO(2) samples are shown in Figure 5 and also in Figure 8a−e, which will be discussed later in Section III of this article. Like the absorption spectrum, this UV band undergoes a blue shift with decrease of the particles size. Additionally, we have found another UV fluorescence band at 300 ± 10 nm. These two UV bands were present in almost all measured spectra whatever the preparation method: in ZnO(1) or ZnO(2) samples. But in contrast to the *band gap* emission the more short-wave 300-nm UV band undergoes no shift with cluster size. Moreover, we have not observed any fluorescence below 280 nm (and up to λ_{exc} = 248 nm). We have concluded that it belongs to the *smallest primary particles* (or monomers), which are always present in solutions, at least until clusters grow. Our conclusion is in agreement with previous study,[10] where the most short-wave onset of absorption has been observed at 306 nm, which has been associated with a particle size below the TEM resolution $D \leq 0.5$ nm. A similar conclusion about the HOMO−LUMO character of the 275-nm transition observed in an absorption of freshly prepared ZnO colloids (~200 molecules) has been made in ref 12.

In contrast to the UV spectra, visible fluorescence spectra of ZnO particles were sensitive to the preparation procedure (and, therefore, to environmental conditions). Some examples of fluorescence spectra recorded in ZnO(1) and ZnO(2) samples are shown in Figure 5. The well-known green fluorescence at $\lambda_{fluo}^{(1)} = 510 \pm 50$ nm appeared in ZnO(1) samples. On the other hand, a new blue band at $\lambda_{fluo}^{(2)} \approx 430$ nm has been observed in ZnO(2) samples. With its presence the 510-nm band was strongly suppressed. Both bands undergo a red shift with an increase of the particle size. But this shift was less pronounced than that of the UV band gap transitions (measured by the onset of the absorption spectra). For example, in freshly prepared colloids (which contain ~3 nm particles), the visible band was shifted only by ~50 meV (10 nm) to the red from the solid-state spectrum ($\lambda_{max}^{solid} = 520$ nm at $t \rightarrow \infty$). In the same time the onset of the absorption spectrum was shifted by 300 meV to the blue. No indication of the blue 430-nm fluorescence in the solid state exists in literature.

We shall now discuss the nature of the visible fluorescence bands. Two concepts have been proposed in literature: the concepts of "anion vacancies"[23] (ZnS, ZnO) and of "charged traps" (CdS).[24] According to the first concept, positive Zn^{2+} ions adsorbed at the carrier particle promote visible fluorescence by deforming interatomic bonds. In the second concept fluorescence belongs to a radiative recombination of $e^- - h^+$ trapped in two preexisting distant traps: Tr^+ and Tr^-. Although an indication of the first model has been given in ref 9, the second model has been preferentially adopted later in ref 10 for ZnO particles. Nevertheless, we could not accept the second model for the visible band interpretation for several reasons. (i) Actually, clusters are very small objects with a large surface-to-volume ratio. For example, in ~3 nm ZnO particles roughly 50% of molecules are at the surface: $N_{surf}/N_{vol} \approx (S \cdot R_0)/(V - S \cdot R_0) = (3R_0)/(R - 3R_0) = 0.5$ (here S and V are, respectively, the cluster surface and volume, and we accept $R_0 = 1.8$ Å as an intermolecular distance). Therefore, the concept of surface fluorescence centers seems to be more realistic for nanoparticles. Sensitivity of the fluorescence spectra to environmental conditions speaks in favor of this hypothesis. (ii) The $e^- - h^+$ recombination from $Tr^+ - Tr^-$ traps supposes a restoration of an intertrap Coulomb field after the transition. The field is originally screened by the $e^- - h^+$ couple. In the unexcited nanoparticle, an environmental dielectric relaxation will lead to a $Tr^+ - Tr^-$ energy lowering with a particle size growth (the ground state). On the contrary, this is not the case of the excited state, which is neutral. This should result in a blue shift of corresponding spectra when nanoparticles grow, which is in contrast with experimental observations. (iii) The second model has been developed to explain the faster decay of the short-wave component of inhomogeneous broad-band fluorescence spectra of CdS nanoparticles. No such $\lambda_{fluo}^{(max)}(\tau_{fluo})$ dependence is known in literature for ZnO clusters. On the other hand, in the present study we have observed a long fluorescence decay in ZnO particles, presented in Figure 6. The sample has been

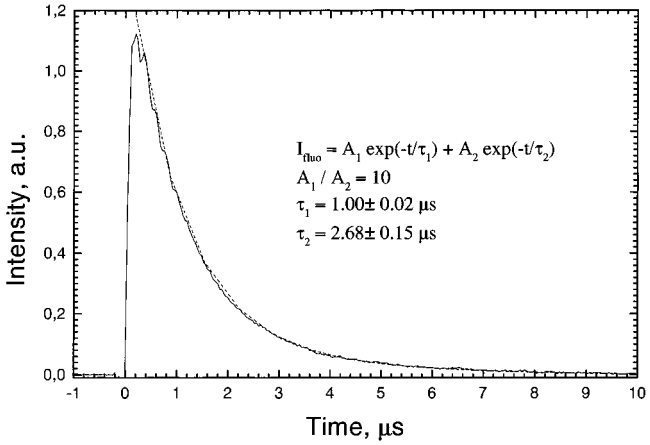

Figure 6. Fluorescence decay in ZnO(1) nanoparticles ([ZnO] = 4×10^{-3} M).

prepared by the first method with Zn^{2+} excess and [ZnO] = 4×10^{-3} M. Particles size could be estimated as $2R_{particle} \approx 4$ nm. In contrast to previous observations, we have found an almost monoexponential fluorescence decay with a lifetime $\tau_{fluo} \approx 1.0$ μs. Additionally, recording time-gated visible spectra with delays of $\Delta t = 0$, 50, and 300 ns after the excitation laser pulse we have found no difference between them. To our mind this can be an indication of a nonstatistical nature of the green fluorescence emission.

We believe that in small ZnO nanoparticles like our clusters, the surface states promoted by excess Zn^{2+} ions are responsible for the green fluorescence. The idea about the nanocrystallites fluorescence has been recently developed in ref 25. In this article the existence of molecular self-trapped excitons (m-STE) at some surface bonds has been shown from total energy calculation on the example of silicon nanocrystallites. It has been found that a bond deformation is responsible for this effect, which is likely a general feature for semiconductor clusters. We used this idea for an estimation of bond length deformation in the ZnO molecule. First, we have approximated the ground state of ZnO by Morse potential (see, e.g., ref 26). Dissociation energy ($D'_e = 5$ eV), vibrational quantum ($\omega'_e = 635$ cm^{-1}), and equilibrium internuclear distance ($r'_e = 1.80$ Å) have been chosen by analogy with other metal oxides. Second, a double-minima parabolic excited-state potential has been considered; the first short-range branch is similar to the ground-state curve, and the second long-range branch has to be adjusted. The interband transition energy has been adjusted to 3.44 eV between the ground and short-range excited potentials. After that, the energetic position of the long-range branch of the excited potential was fitted to reproduce the shape of the fluorescence spectrum. The result of this calculation is shown in Figure 7. The best fit was achieved with a bond length increase by $\Delta r = 0.33$ Å, that is, by 18% respectively to the ground-state equilibrium distance.

Moreover, this idea appears to be useful in treatment of the visible band red shift with cluster size. We have used a very simple model of a dielectric sphere of cluster radius R_{cl} ($\epsilon_{ZnO} = 3.7$), polarized by a static dipole of ZnO molecule ($d = qr$). We take into account a permanent dipole−induced dipole interaction. The electric field of a free dipole is

$$\bar{E}_{dip} = \frac{3\bar{r}(\bar{d}\bar{r}) - \bar{d}(\bar{r}\bar{r})}{r^5} \qquad (1)$$

It creates induced dipoles at $\bar{r}$ with $\bar{d}_{ind} = \alpha \bar{E}_{dip}$, where α is the medium polarization. Integration of induced dipoles electric

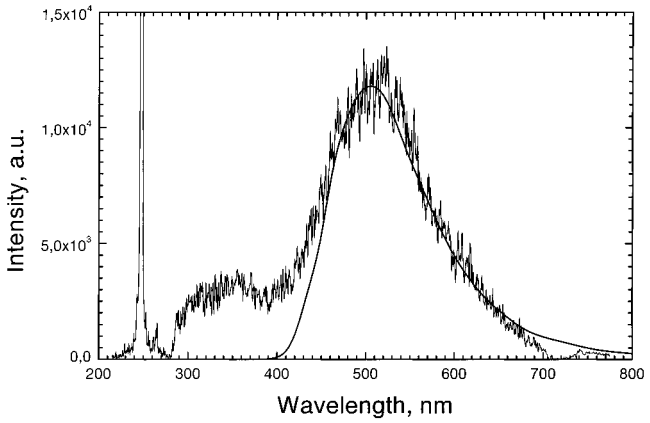

Figure 7. Experimental and fitted spectra of the green emission of ZnO nanoparticles (for explanation, see text)

fields at the permanent ZnO dipole position $\bar{r} = 0$ gives us an interaction energy. To avoid a singularity at $\bar{r} = 0$ and to relate the dipole energy to its energy in the solid, we have carried out an integration in the excluded volume, that is, from infinity and until the cluster sphere

$$U_{dip} = \int_V^\infty \bar{d} \frac{3\bar{r}(\bar{d}_{ind}\bar{r}) - \bar{d}_{ind} r^2}{r^5} \frac{dV}{V_0} \qquad (2)$$

(here V_0 is the unitary molecular volume). We have considered the ground and excited states dipole moments of an ionic $Zn^{2+} - O^{2-}$ molecule as $d_g = 2er''_e$ and $d_{exc} = 2er'_e$ respectively. Here we have to note that because of a larger dipole moment of the excited state (as has been found, $r''_e < r'_e$) the dielectric relaxation of the excited state is stronger and the total effect results in an energy decrease with cluster growth. To calculate the spectral shift measured in the experiment, we have to take the difference between the excited- and ground-state integrals in the form of (2). Finally, we obtain

$$\Delta E_{ZnO} = \frac{8(\epsilon - 1)e^2(r'^2_e - r''^2_e)}{3R^3_{cl}} \qquad (3)$$

Substituting the known values of ϵ and r''_e and the fitted value of r'_e in (3), we find a numerical relation: $\Delta E_{ZnO} = 131 R_{cl}^{-3}$ in meV for R_{cl} expressed in nm.

The formula gives an energetic shift of the green continuum for the smallest clusters of 3 nm observed in our experiments (respectively to the solid-state emission) to be equal to 40 meV or 8 nm, which is in agreement with our observations. Moreover, the largest spectral shift of this band of 60 nm (~300 meV) observed in ZnO nanoparticles in ref 10 according to (3) corresponds to the size of 1.5 Å. This is in agreement with experimental TEM histograms measured in refs 10 and 11.

To quantitatively verify the model, it is very interesting to follow the time-resolved spectra with nanosecond time resolution in smaller particles, ~1-2 nm. Potentially, lifetime shortening with cluster size decrease belongs to a *molecular domain* feature of cluster size. This effect has been recently found in Kr_N clusters[27] (in molecular physics language this m-STE state corresponds to an excited krypton dimer in the lowest $1_u/0_u^-$ state localized in a distorted solid structure). This model also explains that the more short-wave emission with a shorter lifetime originates from smaller clusters.

The proposed simple model can explain why Zn^{2+} ions promote visible fluorescence. Actually, if the ions attach to

the cluster surface, an easily deformed bond is produced. On the other hand, crystalline structure stabilization forces could prevent a particular bond distortion through a potential barrier. Therefore surface m-STE localization seems to be preferential at least in nanocrystallites. When particles grow, the probability of the surface m-STE localization decreases in agreement with a decrease of the surface-to-volume ratio (S/V), and the total recombination rate that leads to the visible emission $w^{rad} = S{\cdot}k_{surf} + V{\cdot}k_{vol}$ decreases in a favor of a nonradiative recombination w^{nrad} (we suppose that $k_{surf} \gg k_{vol}$). This effect can explain the maximum quantum yield of the green fluorescence (LQY = $w^{rad}/(w^{rad} + w^{nrad}) \approx 16\%$) reported in ref 10, which has been attained during the growth of ZnO nanoparticles, when the absorption onset passed ~330 nm.

According to our assignment of the green fluorescence band at 510 nm, the blue 430-nm band that appears in solutions with an excess of OH^- ions also belongs to surface centers. Apparently, the molecular structure of this m-STE is complex and involves the anionic OH^- group. We have to note that the green continuum could be seen in these spectra too, but its intensity is low. In the limit of high OH^- concentrations, it may originate from the m-STE's localized in a cluster volume. By analogy with the above discussion and if our supposition is true, the ratio of the green-to-blue continua intensities should increase with Zn^{2+}/OH^- concentration ratio, which has to be verified. This band identification is currently in progress.

Finally, at a long time after the preparation an additional sharp emission band appeared in some Zn^{2+}-rich colloids at 545 nm (see Figure 5d). Its nature is not clear, although it might be due to impurity traces or to some structural reorganization of particles.

III. Particle Size Distribution. Now we will discuss the possibility of recovering the particle size distribution from the spectroscopic experiment. It is of importance in view of potential applications that need an in situ control of particle growth.

Mean cluster size could be principally derived from the absorption onset measurements if we would obtain the true $R(\lambda_{AO})$ calibration curve. Here, there are some questions to resolve both in theory and in experiment. Theoretical modeling needs to overcome (1) the effective mass approximation and problems of changes (2) in the dielectric constant and (3) in the cluster structure with size. Experimental information about a cluster size distribution is generally available from transmission electron microscopy (TEM). However, because of a special sample preparation for TEM measurements, this method is a rather indirect one. A copper mesh covered with a carbon film and activated by UV radiation is used as a sample holder. Adhesion of nanoparticles to the film occurs during the time when a drop of a colloidal solution is placed on it (typically ~30 s). It is assumed that the particle size distribution on the film and in the solution is the same. Other measurements are needed to experimentally verify this assumption. Additionally, absorption measurements could be validated for a relatively narrow size distribution curve *N(R)*. In more general case transmission intensity depends on *N(R)*: $I_\lambda^t = I_\lambda^0{\cdot}\exp(-\int_{all\ R}\sigma_\lambda(R)lN(R)\,dR)$, and a solution of the inverse problem becomes difficult. Therefore, approaches from both (modeling and experiment) sides could be important.

Utilization of our calibration curve (curve d in Figure 1a) has allowed us to trace a $R_{particle}(t)$ dependence in Figure 4. The fit of experimental data of particle size evolution in time presented in Figure 4 results in $R_{particle} \propto t^{1/3}$. This might correspond to a slow compact aggregation in terms of ref 22. In this mode cluster grows as a dense 3D object by addition of primary particles (or monomers). Below we will use fluorescence spectra measurements to verify this supposition. In fact, the growth mechanism is presently unknown and could be rather complicated. Addition of primary particles to the cluster could proceed as a surface-catalyzed reaction. We will not discuss this chemistry in the present article.

In contrast to the mean size, cluster size distribution is difficult to extract from absorption measurements. We believe that fluorescence lifetime and spectral studies could help in this respect. Below we will discuss which information could be accessible from the UV fluorescence spectra. To obtain the net UV spectrum, in each case we have fitted the accompanying visible continuum by a Gaussian-shaped curve $I(\nu)$ and we have subtracted this fit from the total spectrum. Examples of these net UV spectra are given in Figure 8a−e.

Actually, ZnO clusters of different sizes contribute to the UV fluorescence

$$I_{fluo}(\lambda) = \int_R W_{exc}(R)\, W_{fluo}(\lambda, R)\, f(R)\, dR \qquad (4)$$

where $W_{exc}(R)$, $W_{fluo}(\lambda, R)$, and $f(R)$ are the excitation and fluorescence efficiencies and the size distribution function. (i) As has been shown in theoretical work,[28] the absorption coefficient in a direct-band semiconductor with the ratio $m_h/m_e \leq 1.9$ diverges as $1/R^3$ in the region of a strong confinement ($R < a_B$), and increases as R^3 in the region of a weak confinement ($R > a_B$) as the size of the nanocrystal increases. ZnO is a direct-band semiconductor with $m_h/m_e \approx 1.9$ and $a_B = 1.25$ nm. In the range of particle sizes under study ($1 \leq R/a_B \leq 5$), we have approximated the excitation efficiency by $W_{exc} \propto R$.[28] (ii) The fluorescence efficiency depends on rates of radiative (τ_{rad}^{-1}) and nonradiative (k) losses as $W_{fluo} \propto \varphi_R^\lambda\{\tau_{rad}^{-1}/(\tau_{rad}^{-1} + k)\}$ (here φ_r^λ is a fluorescence line shape for a fixed R). We have approximated the rate of the exciton radiative transitions by $\tau_{rad}^{-1} \propto R^2$ in the range of particle sizes under investigation. On the other hand, we relate nonradiative losses with a surface quenching ($k \propto S_{particle}$). In light of the finding of ref 10 that the UV emission decay time is shorter than 100 ps, the quenching is dominant ($k \gg \tau_{rad}^{-1}$), and one can consider $W_{fluo}(\lambda, r) \propto \varphi_R^\lambda$. Therefore, we rewrite (4) as

$$I_{fluo}(\lambda) \propto \int_R f(R)\varphi_R^\lambda R\, dR \qquad (5)$$

In this expression the function φ_R^λ relates two distributions: $f(R)$ and $I_{fluo}(\lambda)$, abscissas of which are coupled by the calibration curve $\lambda(R)$ (curve d in Figure 1a). To convert the experimentally measured $I_{fluo}(\lambda)$ into $f(R)$ we make some simplifications: (1) we suppose the width of φ_R^λ ($\Delta\lambda_{1/2}$) to be much narrower than $f(R(\lambda))$, and (2) we consider that $\Delta\lambda = (d\lambda/dR)\Delta R$, that is, the first derivative λ'_R to be constant over the range of $(\lambda \pm \Delta\lambda_{1/2})/2$ (in this sense $\Delta\lambda_{1/2}$ determines the resolution of the method). The above assumptions allows one to transform (5) into

$$I_{fluo}(\lambda) \propto f(R)R\frac{dR}{d\lambda}\int\varphi_R^\lambda\, d\lambda = f(R)R\frac{dR}{d\lambda}$$

Finally, we obtain the solution of the inverse problem of the size distribution recovery from fluorescence spectral measurements

$$f(R) \propto I_{fluo}(\lambda){\cdot}\frac{1}{R}\frac{d\lambda}{dR} \qquad (6)$$

For the calculation of the factor $d\lambda/dR$, we have used the

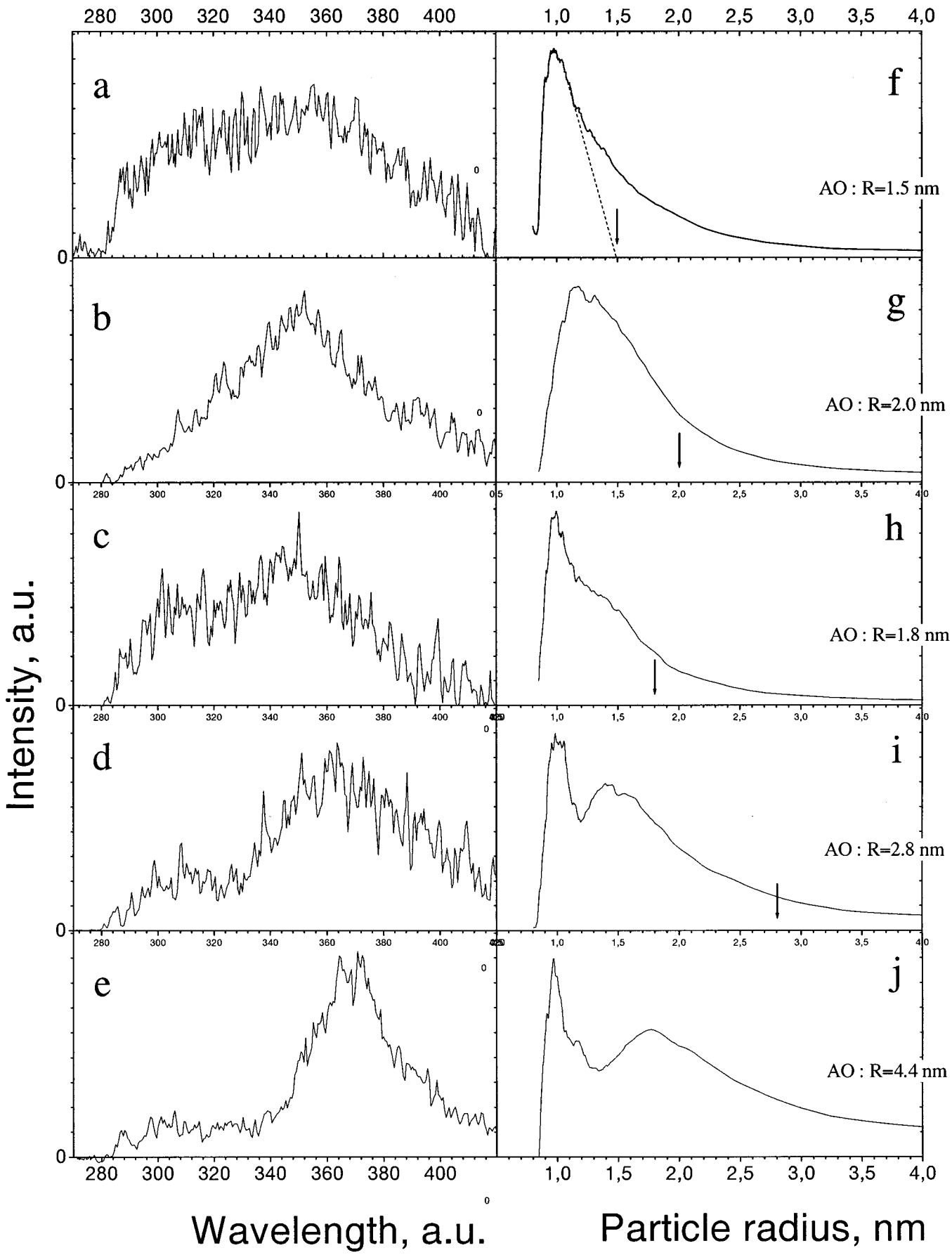

Figure 8. UV fluorescence spectra (a−e) and particles size distribution, extracted from the spectra (corresponding pairs are arranged in rows). Spectra were recorded in ZnO(1) sample 1, 5, 5, 11, and 42 days after preparation. The second and the third rows present the results 5 days after preparation before and after the microwave treatment of the samples. Particles sizes obtained from the onset of absorption spectra are also indicated in the figure (AO).

calibration curve d from Figure 1a, and we assume a constant Stokes shift (of absorption-to-fluorescence transitions in particles of a given R) of $\sim 10^2$ meV is followed throughout the entire spectral range of nanoparticle interband transitions: 300−380 nm. As we already stated, the line shape factor ϕ_R^λ imposes alimitation on the applicability of the analytical solution (5): $\lambda_{\text{solid}} - \lambda_{\text{particle}}(R) \geq \Delta\lambda_{1/2}/2$. Practically, for $\Delta\lambda_{1/2} \approx 10$ nm this sets a limit of $R_{\text{particle}} \leq 5$ nm. Cluster size distributions built up by using the formula (5) are shown in Figure 8f−j. The corresponding pairs of UV spectrum/size distribution are given in the rows in Figure 8.

An interesting feature of the particle growth kinetics is the appearance of the second maximum in the distribution function after some time (∼4 days) from the beginning of the process. Its position is always at a smaller radius than the "mean" size determined from absorption onset measurements (AO), which is also indicated in each curve by an arrow. It is very interesting to note that the same tendency has been found in refs 9−11: the maxima of TEM histograms of various ZnO samples appeared to correspond ∼25% smaller particles than has been measured by AO. An attempt to rationalize this disagreement has led the authors of ref 12 to a conclusion that it might be due to a particle aggregation, which has not been taken into account in the theoretical models. They have proposed that aggregation dominates even in highly diluted solutions. However, we believe that it is not the case at least in our experiment. Comparison of two sets of measurements (b, g) and (c, h) presented in Figure 8, which were taken respectively, before and after an intense ultrasound treatment of the sample, evidences only a minor change in the absorption onset energy. The only difference is the change of the peak intensities of the observed bimodal particle size distribution. We conclude that the aggregation, if it takes place, influences only the spectral intensity but not the absorption onset frequency.

We believe that the first maximum relates to the smallest primary particles, which are always present (or which being generated) in the solution. According to our measurements that radius corresponds to $R \leq 1$ nm. With time, the relative number of large particles increases, which is manifested as a growing tail of the distribution curve. The second maximum may indicate a "flocculation regime" of the growth kinetics. In terms of the Smoluchowski equation this corresponds to the case of the homogeneity factor $\omega < 0$, if we suppose that the aggregation rate constant scaling obeys a homogeneous relation $K_{\lambda i,\lambda j} = \lambda^{2\omega} K_{i,j}$.[22] This means that growth rates $K_{i,j}$ should decrease with particle size, the reason of which is not yet clear. Nevertheless, if we accept such hypothesis the number of molecules in the cluster, which corresponds to the maximum of the distribution curve $N_{\max}$, can be related to the mean number ⟨N⟩ by

$$N_{\max} = \frac{2\omega}{2\omega - 1} \langle \mathrm{N} \rangle \tag{7}$$

for sufficiently large clusters, ⟨N⟩ ≫ 1. If we remember now that $R_{\text{particule}} \propto t^{\gamma/d_f}$ (where $\gamma^{-1} = 1 - 2\omega$ and d_f is the fractal dimension) and that our measurements have given the power factor of $^1/_3$ (see Figure 4), one can readily reduce (7) to

$$R_{\max} = (1 - d_f/3)^{1/d_f} \langle \mathrm{N} \rangle^{1/d_f} \tag{8}$$

We tentatively assign the particle size determined from absorption onset measurements to the mean size in the sense $\langle R \rangle \propto \langle N \rangle^{1/d_f}$ and plot it versus $R_{\max}$ in Figure 9. Linear least-squares fit of the experimental data results in the factor

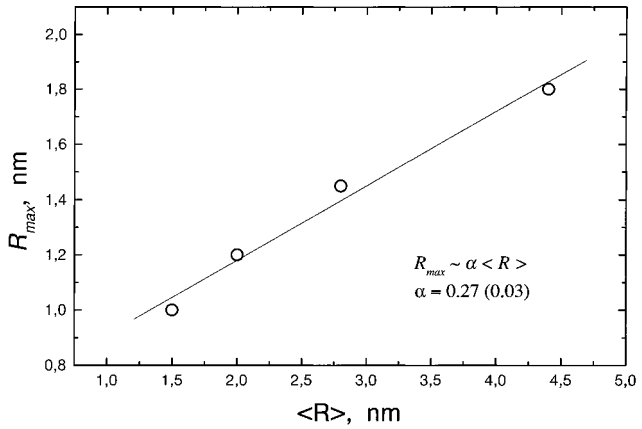

Figure 9. Dependence of the particle size corresponding to the distribution curve maximum $N_{\max}$ (determined from the fluorescence spectra measurements) on the "mean" cluster size ⟨N⟩ (determined from the absorption onset measurements) for different moments of time after the ZnO(1) sample preparation.

$$(1 - d_f/3)^{1/d_f} = 0.27 \pm 0.03 \tag{9}$$

Using (9) we have obtained the homogeneity factor of $2\omega = -2.4 \times 10^{-2}$ and the fractal dimension of the nanoparticules under study $d_f \approx 2.93$. In fact, the ZnO nanoparticles grow as compact objects, which agrees with our initial supposition.

Particles growth kinetics as well as the fractal structure strongly depend on $K_{i,j}$'s. In case of inhomogeneous kinetics rates, the general conclusion conserves that $K_{i,j}$'s decrease with particle radius, at least in a certain range of size. This effectively creates a "bottleneck" of the relaxation scheme and a particle accumulation burst on the distribution curve, moving in time, like we have experimentally observed. This is consistent with the classical DLVO theory, where an increase of an activation barrier with a size of aggregating particles has been predicted (see, e.g., ref 29). Another factor whose consequence on the growth mode has not been explicitly verified at the present is the source of primary particles. This work is in progress.

Conclusion

In the present work we have performed a spectroscopical study of the initial stage of the colloidal ZnO particles growth. Colloids were prepared in different environments: with excess Zn^{2+} or OH^- ions. In fluorescence spectra we have observed three principal bands: (1) the UV band in the range between 280 and 380 nm, (2) the 430-nm blue band characteristic of solutions with OH^- excess ions, and (3) the 510-nm green band, which was the most intense in solutions with Zn^{2+} excess ions. We assign the green band to the m-STE emission due to a distorted Zn − O bond by 18%. In small clusters it is more probable to find these fluorescence centers at the surface. We explain the red shift of the green band with time as a dielectric effect of the growing cluster on the trapped radiating dipole. The UV band has been assigned to the *band gap* fluorescence of clusters of different sizes. This allows us to reconstruct the size distribution curves of growing particles for different moments of time. The distribution curves display two maxima tentatively assigned to the smallest primary particles or monomers and to the growing ones. Comparison of the maximum in the size distribution with a "mean" size obtained from the absorption onset measurements can clarify the reaction kinetics. Supplementary to the spectral measurements, we expect to apply the lifetime measurements of nanoparticle samples. It could

be very interesting because of the high sensitivity of the wave function to the particle size.

References and Notes

(1) Alivisatos, A. P. *Science* **1996**, *271*, 933.
(2) Wang, Y.; Herron, N. *J. Phys. Chem.* **1991**, *95*, 525.
(3) Gaponenko, S. V. *Semiconductors* **1996**, *30*, 315.
(4) Andres, R. P.; Averback, R. S; Brown, W. L.; Brus, L. E.; Goddard, W. A.; Kaldor, A.; Louie, S. G.; Moscovits, M.; Peercy, P. S.; Riley, S. J.; Siegel, R. W.; Spaepen, F.; Wang, Y. *J. Mater. Res.* **1989**, *4*, 704.
(5) Brus, L. E. *J. Chem. Phys.* **1983**, *79*, 5566.
(6) Brus, L. E. *J. Chem. Phys.* **1984**, *80*, 4403.
(7) Brus, L. E. *J. Phys. Chem.* **1986**, *90*, 2555.
(8) Henglein, A. *Top. Curr. Chem.* **1988**, *143*, 113.
(9) Koch, U.; Fojtik, A.; Weller, H.; Henglein, A. *Chem. Phys. Lett.* **1985**, *122*, 507.
(10) Bahnemann, D. W.; Kormann, C.; Hoffmann, M. R. *J. Phys. Chem.* **1987**, *91*, 3789.
(11) Haase, M.; Weller, H.; Henglein, A. *J. Phys. Chem.* **1988**, *92*, 482.
(12) Spanhel, L.; Anderson, M. A. *J. Am. Chem. Soc.* **1991**, *113*, 2826.
(13) See, e.g.: Smith, R. A. *Semiconductors*, 2nd ed.; Cambridge: London, 1978.
(14) Urbach, F. *Phys. Rev.* **1953**, *92*, 1324.
(15) Enright, B.; Fitzmaurice, D. *J. Phys. Chem.* **1996**, *100*, 1027.
(16) Kayanuma, Y. *Solid State Commun.* **1986**, *59*, 405.
(17) Weller, H.; Schmidt, H. M.; Koch, U.; Baral, S.; Henglein, A.; Kunath, W.; Weiss, K.; Dieman, E. *Chem. Phys. Lett.* **1986**, *124*, 557.
(18) Nozik, A. J.; Memming, R. *J. Phys. Chem.*, **1996**, *100*, 13061.
(19) Fojtik, A.; Weller, H.; Koch, U.; Henglein, A. *Ber. Bunsen-Ges. Phys. Chem.* **1984**, *88*, 969.
(20) Krishna, M. V. R.; Friesner, R. A. *J. Chem. Phys.* **1991**, *95*, 8309.
(21) Wang, Y.; Suna, S.; Maher, W.; Kasowski, R. *J. Chem. Phys.* **1987**, *87*, 7315.
(22) Jullien, R.; Botet, R. *Aggregation and Fractal Aggregates*; World Science: Singapore, 1987.
(23) Weller, H.; Koch, U.; Gutiérrez, M.; Henglein, A. *Ber. Bunsen-Ges. Phys. Chem.* **1984**, *88*, 649.
(24) Chestnoy, N.; Harris, T. D.; Hull, R.; Brus, L. E. *J. Phys. Chem.* **1986**, *90*, 3393.
(25) Allan, G.; Delerue, C.; Lannoo, M. *Phys. Rev. Lett.* **1996**, *76*, 2961.
(26) Herzberg, G. *Spectra of Diatomic Molecules*, 2nd ed.; D. van Nostrand: New York, 1966.
(27) Kanaev, A. V.; Museur, L.; Castex, M. C. *J. Chem. Phys.* **1997**, *107*, 4006.
(28) Kayanuma, Y. *Phys. Rev. B* **1988**, *38*, 9797.
(29) Hiemenz, P. C. *Principles of Colloid and Surface Chemistry*, 2nd ed.; Marcel Dekker Inc.: New York, 1986.